A Low-Cost Synchronized PPG-PCG IoT System for Arterial Stiffness Risk and Cuffless Blood Pressure Estimation

1st Avignya Gautam
Department of Electronics and Computer Engineering
Thapathali Campus (Tribhuvan University)
Kathmandu, Nepal
gautamavignya@gmail.com

2nd Agrima Shahi
Department of Electronics and Computer Engineering
Thapathali Campus (Tribhuvan University)
Kathmandu, Nepal
thakuriag61@gmail.com

3rd Kripa Timalsena
Department of Electronics and Computer Engineering
Thapathali Campus (Tribhuvan University)
Kathmandu, Nepal
kripatimalsena11@gmail.com

4th Bibash Adhikari
Department of Electronics and Computer Engineering
Thapathali Campus (Tribhuvan University)
Kathmandu, Nepal
adhikaribibash43@gmail.com

5th Umesh Kanta Ghimire
Department of Electronics and Computer Engineering
Thapathali Campus (Tribhuvan University)
Kathmandu, Nepal
ukg@tcioe.edu.np

***Abstract*—Cardiovascular diseases (CVD) demand accessible early-screening tools, yet standard arterial stiffness and blood pressure (BP) assessments rely on costly, operator-dependent equipment. This paper presents a low-cost, portable Internet of Things (IoT) sensing prototype and computational pipeline for non-invasive cardiovascular screening using synchronized Photoplethysmography (PPG) and Phonocardiography (PCG). An ESP32 microcontroller running FreeRTOS ensures microsecond-level synchronization between an optical MAX30102 sensor and a custom four-stage analog-conditioned piezoelectric transducer. To mitigate acoustic sensor noise and age-related pulse morphology variations, a cross-modal physiological gating technique and inflection-anchored fiducial detection algorithms are introduced. Twelve extracted hemodynamic features, including Pulse Arrival Time (PAT) and Subendocardial Viability Ratio (SEVR), were evaluated using an eXtreme Gradient Boosting (XGBoost) framework. To account for hardware timing jitter and measurement uncertainty, models were trained and benchmarked in-silico on 4,328 virtual subjects from the Pulse Wave Database (PWDB) augmented with parameter-specific Gaussian noise. Benchtop frequency-domain characterization confirmed that the analog front-end suppresses broadband interference above 150 Hz, while on the held-out test set ($n = 866$), the XGBoost pipeline achieved 91.22% accuracy (0.9826 macro ROC-AUC) for arterial stiffness risk classification and estimated systolic/diastolic BP with Mean Absolute Errors of 3.86/3.06 mmHg.**

***Index Terms*—Photoplethysmography (PPG), Phonocardiography (PCG), Cuffless Blood Pressure, Arterial Stiffness, Internet of Things (IoT), Machine Learning, Cross-Modal Sensor Fusion.**

I. Introduction

Cardiovascular disease (CVD) remains the leading cause of mortality globally, disproportionately affecting low- and middle-income countries such as Nepal due to restricted access to early diagnostic facilities [1], [2]. Arterial stiffening—a primary precursor to hypertension and heart failure—develops long before visible clinical symptoms manifest [3]. The clinical gold standard for assessing arterial stiffness is Carotid-femoral Pulse Wave Velocity (cfPWV); however, traditional cfPWV and cuff-based oscillometric blood pressure (BP) measurement systems are expensive, require trained operators, and are unsuitable for continuous monitoring [4].

Recent advancements in wearable instrumentation have popularized Photoplethysmography (PPG) for non-invasive monitoring [5], [6]. Yet, single-modality PPG systems lack the temporal grounding provided by a cardiac reference channel, making it impossible to independently resolve Pulse Arrival Time (PAT) or Left Ventricular Ejection Time (LVET) for accurate stiffness and BP estimation [5], [7]. While incorporating Phonocardiography (PCG) solves this temporal deficit by capturing mechanical heart valve closures, utilizing low-cost piezoelectric discs introduces broadband noise susceptibility and synchronization challenges on resource-constrained microcontrollers. Furthermore, morphological feature extraction often fails in older subjects when reflected arterial waves merge into the primary systolic upstroke.

To address these limitations, this paper proposes an afford-

able dual-sensor IoT hardware architecture paired with a noise-augmented machine learning pipeline:

- **Fault-Tolerant Dual-Core Hardware Architecture:** A FreeRTOS implementation on an ESP32 achieving microsecond-level synchronization between an optical MAX30102 sensor and an LM324-conditioned piezoelectric transducer, fabricated for under NPR 5,210 ($\sim$\$38 USD).
- **Cross-Modal Gating and Morphology-Aware Extraction:** An algorithm that utilizes the PPG signal to temporally bound PCG heart-sound envelopes, paired with derivative-inflection fallback heuristics to isolate fiducial landmarks across aging pulse morphologies.
- **Noise-Augmented In-Silico ML Benchmark:** An XGBoost inference pipeline benchmarked against Random Forest and Gradient Boosting across 4,328 virtual subjects from the Pulse Wave Database (PWDB) [8] augmented with synthetic hardware jitter.

II. Background and Related Work

A. Arterial Stiffness and Pulse Wave Velocity

The relationship between arterial compliance and pressure wave propagation is governed by the Moens-Korteweg equation, $\text{PWV}^2 = (E \cdot h)/(2 \cdot r \cdot \rho)$, where E is the arterial wall elastic modulus, h is wall thickness, r is luminal radius, and ρ is blood density [9]. Clinical literature establishes that an increase in aortic PWV of 1 m/s is associated with a 14–15% higher risk of cardiovascular events [3]. By capturing mechanical heart valve closures (PCG) and the arrival of the peripheral blood volume pulse at the digital artery (PPG), PAT and LVET can be extracted as strong surrogates for central PWV [7].

B. Non-Invasive Cardiovascular Monitoring

Prior research has demonstrated the feasibility of fusing PCG and PPG for vascular assessment. Margain et al. utilized PCG-derived cfPWV to establish temporal references for the S2 heart sound, achieving strong correlations with arterial age and intraclass correlation coefficients of 0.75–0.90 [10]. However, existing literature primarily relies on clinical-grade microphones. Transitioning these methodologies to low-cost piezoelectric discs introduces broadband interference and motion artifacts that static filters fail to isolate.

C. Machine Learning in Hemodynamics

Tree-based ensemble models are increasingly applied to map PPG morphologies to vascular metrics [11]. However, models trained strictly on pristine simulated datasets suffer from domain shift when exposed to I^2C bus jitter and low-cost sensor arrays [7]. This work distinguishes itself by combining inflection-anchored feature extraction with bounded Gaussian noise injection and physiological bounding heuristics.

III. Hardware and System Architecture

The portable unit operates on a dual-core DOIT ESP32 DevKit V1 microcontroller (240 MHz) running FreeRTOS, powered by a 1200 mAh LiPo battery with a TP4056 charger and XL6009E1 5 V boost converter. The partitioned system architecture is illustrated in Fig. 1.

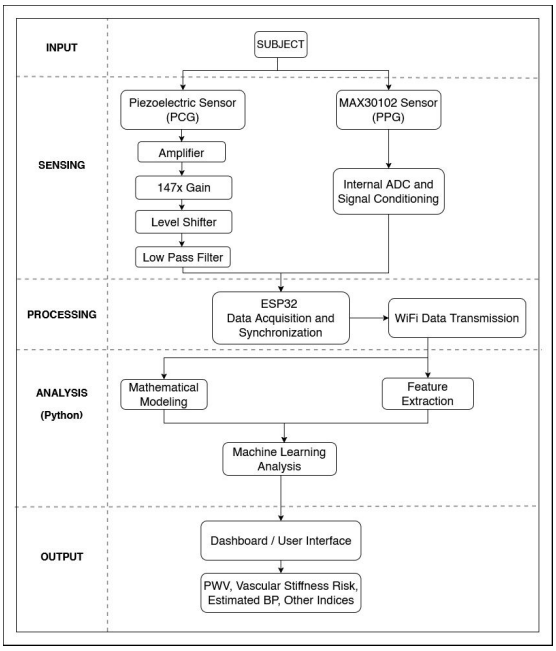

Fig. 1. System block diagram illustrating the dual-sensor acquisition, LM324 analog signal conditioning, and ESP32 MQTT telemetry pipeline.

A. Signal Acquisition and Conditioning

Fingertip optical blood volume pulsations are captured via I^2C at 125 Hz using a MAX30102 module (660 nm red and 880 nm IR LEDs, 18-bit ADC). Simultaneously, chest-wall heart sounds are detected using a 27 mm brass-backed piezoelectric ceramic disc. To condition the high-impedance millivolt AC piezo output prior to 12-bit ADC sampling at 500 Hz (GPIO 34), all four op-amps of a quad LM324 IC are cascaded: (1) a unity-gain buffer with a 10 kΩ divider establishes a 1.65 V mid-supply reference (V_{MID}) to prevent unipolar ADC clipping; (2) a unity-gain differential amplifier with 1 MΩ bridge resistors rejects common-mode electromagnetic noise while forming a 6.3 Hz passive high-pass pole (1 μF coupling capacitor) to attenuate motion drift; (3) an AC-coupled non-inverting stage ($R_f = 82$ kΩ, $R_{in} = 560$ Ω) provides $147\times$ voltage gain; and (4) a critically damped second-order Sallen-Key low-pass filter ($R = 10.56$ kΩ, $C = 100$ nF) enforces a 150 Hz cutoff (-40 dB/decade) before a Schottky diode clamp. The assembled matrix-board prototype is shown in Fig. 2.

B. Fault-Tolerant IoT Telemetry

To prevent Wi-Fi thread-blocking delays from corrupting sample timing, tasks were decoupled across the ESP32 cores:

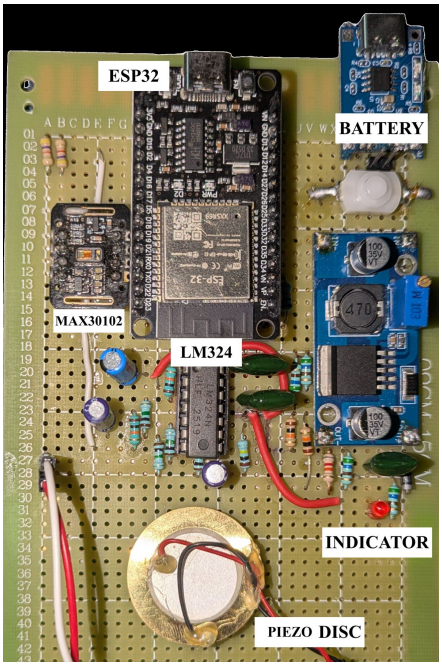

Fig. 2. Matrix-board implementation of the IoT hemodynamic profiler, featuring the ESP32, MAX30102, and LM324 analog conditioning circuit.

Core 1 is strictly dedicated to hardware polling (data producer), servicing sensor interrupts and pushing microsecond-timestamped arrays to a thread-safe FreeRTOS queue. Core 0 operates as the asynchronous network consumer, batching payloads and publishing them to a Mosquitto MQTT broker over Wi-Fi. An auto-recovery watchdog monitors I^2C saturation, applying a 100 ms soft-reset to the MAX30102 upon fault detection without dropping the MQTT socket.

IV. Signal Processing and Feature Extraction

Raw telemetry received by the Python backend is filtered over 10-second windows using a zero-phase fourth-order Butterworth band-pass filter (0.5–18 Hz) for PPG and a fourth-order Butterworth band-pass filter (25–150 Hz) with 50/100 Hz notch filters for PCG, followed by per-cycle min-max normalization to $[0, 1]$.

A. Cross-Modal Physiological Gating

Because piezoelectric transducers are susceptible to ambient noise, identifying S1 and S2 heart sounds via static amplitude thresholds yields high false-positive rates. Instead, the stable optical PPG signal is used to anchor the cardiac cycle. Instantaneous heart rate ($\text{HR} = 60/T_{\text{cycle}}$) derived from PPG systolic peaks establishes dynamic search windows on the PCG Hilbert envelope: valid S1 peaks (T_{S1}) are constrained to occur 210–330 ms prior to the peripheral PPG peak, while systolic duration is bounded by the local R-R interval. Using the maximum second derivative of the PPG upstroke as the arrival trigger ($T_{\text{stop}} = \arg\max \frac{d^2\text{PPG}}{dt^2}$), Pulse Arrival Time and Left Ventricular Ejection Time are resolved as:

$$\text{PAT} = T_{\text{stop}} - T_{\text{S1}}, \quad \text{LVET} = T_{\text{S2}} - T_{\text{S1}} \tag{1}$$

B. Morphology-Aware Fiducial Detection and Bounding

Along with `AGE`, `HR`, `PAT`, and `LVET`, eight morphological features are extracted from each normalized PPG beat: Crest Time (`CT`, foot-to-peak duration), Stiffness Index ($\text{SI} = H/\delta T$), Maximum Upstroke Velocity ($dP/dt_{\text{max}} = \max(\frac{d\text{PPG}}{dt} \cdot f_s)$), systolic area (`PPG_Asys`), diastolic area (`PPG_Adia`), and acoustically gated Subendocardial Viability Ratio (`PPG_SEVR`), where PCG-derived `LVET` defines the exact mechanical boundary of aortic valve closure:

$$\text{PPG_SEVR} = \frac{A_{\text{dia}}}{A_{\text{sys}}} = \frac{\int_{\text{LVET}}^{T_{\text{cycle}}} \text{PPG}(t)\,dt}{\int_{0}^{\text{LVET}} \text{PPG}(t)\,dt} \tag{2}$$

In older subjects with stiffened arteries, reflected waves merge into the systolic downstroke, erasing distinct diastolic peaks. To reliably compute the Reflection Index ($\text{RI} = h_{\text{dia}}/h_{\text{sys}}$), the algorithm locates the steepest systolic drop ($idx_{\text{inf}} = \arg\min d_1[idx_{\text{sys}} : idx_{\text{sys}} + N/3]$) and searches $[idx_{\text{inf}} + 1, 0.80N]$; if no local peak exists in PPG(t), it falls back to the local maximum of the first derivative ($\max d_1$) to capture the inflection plateau. Similarly, the Modified Aging Index is extracted from the second derivative ($d_2 = \frac{d^2\text{PPG}}{dt^2}$) [12]:

$$\text{AGI}_{\text{mod}} = \frac{b - c - d}{a} \tag{3}$$

by bounding the c and d wave searches strictly between the b-wave minimum and diastolic e-wave boundary, utilizing third-derivative zero-crossings ($\arg\min |d_3|$) when inflection waves flatten. If hardware dropouts corrupt a beat, localized median imputation from adjacent valid beats within the 10-second window is applied, defaulting to clinical medians upon full-window failure.

V. Results and Analysis

A. Dataset Preparation and Domain Randomization

Simulated finger PPG waveforms ($f_s = 500$ Hz) and hemodynamic parameters from $N = 4,328$ virtual subjects (aged 25–75 years, after excluding 46 incomplete records) in the PWDB [8] were passed through the Python extraction pipeline. To align vascular Pulse Transit Time (`PTT`) in PWDB with acoustic S1-triggered `PAT`, Isovolumetric Contraction Time was modeled as $\text{ICT} = 45 - 0.15 \times \text{HR}$ (ms) to yield $\text{PAT} = \text{PTT} + \text{ICT}/1000$. To simulate hardware measurement uncertainty and prevent train-serve skew, zero-mean Gaussian noise was injected into the training features: additive jitter of $\sigma_{\text{CT}} = 10$ ms, $\sigma_{\text{LVET}} = 8$ ms, $\sigma_{\text{PAT}} = 5$ ms, $\sigma_{\text{HR}} = 1.5$ bpm, and $\sigma_{\text{RI}} = 0.04$, alongside multiplicative Gaussian noise on AGI_{mod} (15%), dP/dt_{max} (10%), SI (8%), and $A_{\text{sys}}, A_{\text{dia}}$ (5%).

Target labels for arterial stiffness risk were assigned via $\text{RISK} = \max(\text{risk}_{\text{cfPWV}}, \text{risk}_{\text{cPP}})$ adapted from ESC/ESH guidelines [13] ($\text{cPP} = \text{SBP}_a - \text{DBP}_a$): **Low Risk (41.0%):** cfPWV < 8.0 m/s and cPP ≤ 40 mmHg; **Medium Risk (35.7%):** $8.0 \leq$ cfPWV < 9.6 m/s or $40 <$ cPP ≤ 60 mmHg; and **High Risk (23.3%):** cfPWV ≥ 9.6 m/s or cPP > 60 mmHg. The dataset was split 80/20 into a development set ($n = 3,462$, 5-fold cross-validation randomized search) and an unseen held-out test set ($n = 866$).

B. Arterial Stiffness Classification

As shown in Table I, the optimized XGBoost classifier outperformed Random Forest and Standard Gradient Boosting baselines on the held-out test set ($n = 866$), achieving 91.22% accuracy, a macro F1-score of 0.913, and a macro One-vs-Rest ROC-AUC of 0.983. Across 5-fold cross-validation, the model achieved a combined Out-of-Fold (OOF) accuracy of 90.64% ($N = 4,328$, Fig. 3), with misclassifications occurring exclusively between adjacent risk tiers and zero High-Risk subjects misclassified as Low-Risk. Feature importance rankings confirmed that after `AGE`, sensor-derived `RI`, `PAT`, `AGI_mod`, and `CT` contributed the highest gain.

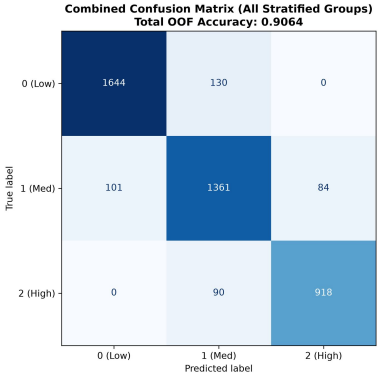

Fig. 3. Combined 5-fold Out-of-Fold confusion matrix of the XGBoost arterial-risk classifier ($N = 4,328$, OOF accuracy: 90.64%; held-out test accuracy: 91.22%), showing zero extreme-class errors.

TABLE I
MODEL PERFORMANCE COMPARISON ON HELD-OUT TEST SET ($n = 866$, MAE IN MMHG)

Model Architecture	Risk Acc.	Risk AUC	SBP MAE	SBP R^2	DBP MAE	DBP R^2
XGBoost	**91.2%**	**0.983**	**3.86**	**0.764**	**3.06**	**0.340**
Random Forest	90.8%	0.980	4.01	0.746	3.15	0.304
Grad. Boosting	89.4%	0.980	3.92	0.758	3.12	0.319

C. Cuffless Blood Pressure Estimation

On the held-out test set ($n = 866$), the XGBoost regressors achieved Mean Absolute Errors (MAE) of 3.86 mmHg (RMSE = 4.73 mmHg, $R^2 = 0.764$) for SBP_a and 3.06 mmHg (RMSE = 3.74 mmHg, $R^2 = 0.340$) for DBP_a (Table I). Although DBP yielded a lower R^2 due to its narrower physiological range (65–90 mmHg), both models satisfied numerical AAMI safety limits (mean error $\leq \pm 5.0$ mmHg, SD ≤ 8.0 mmHg) [14] and achieved British Hypertension Society (BHS) Grade A cumulative error thresholds [15], with 69.86%, 97.46%, and 99.77% of SBP predictions and 80.48%, 99.77%, and 100.0% of DBP predictions falling within ≤ 5, ≤ 10, and ≤ 15 mmHg, respectively. Bland-Altman plots (Fig. 4) confirmed negligible systemic bias for both SBP (-0.08 mmHg, 95% limits: -9.35 to $+9.18$ mmHg) and DBP (-0.04 mmHg, 95% limits: -7.37 to $+7.28$ mmHg).

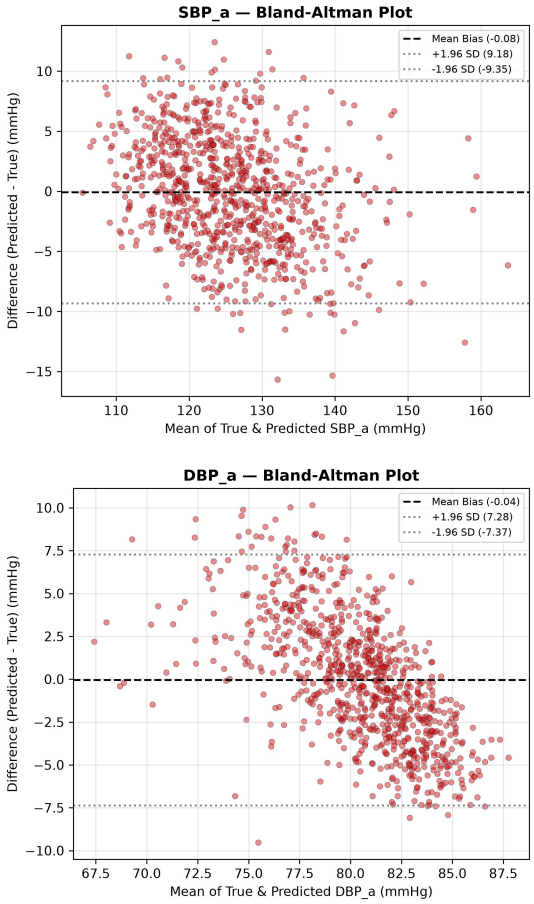

Fig. 4. Bland-Altman plots on the held-out test set ($n = 866$) for (top) SBP_a (mean bias: -0.08 mmHg) and (bottom) DBP_a (mean bias: -0.04 mmHg).

D. Hardware and Signal Conditioning Characterization

To verify the physical prototype's analog conditioning stages and MQTT telemetry pipeline, benchtop frequency-domain characterization was performed using a digital storage oscilloscope alongside live resting signal acquisition. As shown in the unfiltered Fast Fourier Transform (FFT) spectrum in Fig. 5(a), the raw piezoelectric output exhibited broadband interference peaking near 1.067 kHz at -31.2 dBV. After the $147\times$ gain and 150 Hz Sallen-Key low-pass filter, high-frequency noise was attenuated, leaving a dominant 50.33 Hz mains residual at -29.6 dBV (Fig. 5(b)). When placed against chest skin, capacitive coupling elevated the 50 Hz hum to -16 dBV, which was subsequently eliminated by the back-end's 50/100 Hz digital notch filters. During live acquisition, the dual-core ESP32 FreeRTOS pipeline streamed continuous synchronized packets over Wi-Fi without I^2C lockups, cleanly isolating S1/S2 heart-sound envelopes and drift-free PPG systolic peaks.

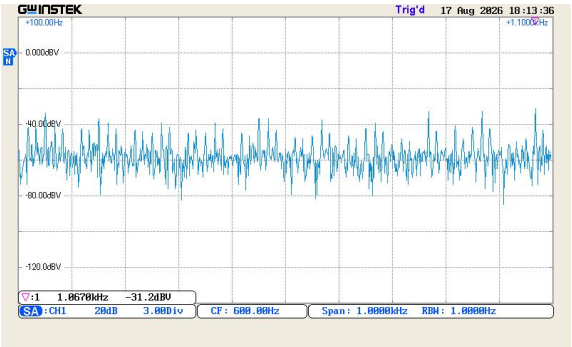

(a) Unfiltered piezo output before Sallen-Key filter.

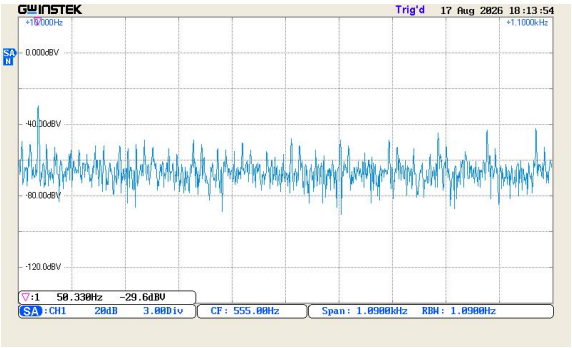

(b) Conditioned PCG spectrum at Sallen-Key filter output.

Fig. 5. Oscilloscope FFT spectrum of the PCG front-end: (a) broadband noise peaking at 1.067 kHz (-31.2 dBV); (b) attenuation of $>$ 150 Hz noise, leaving a 50.33 Hz (-29.6 dBV) residual.

VI. Conclusion and Future Work

This paper presented a low-cost, dual-sensor IoT hardware architecture and morphology-aware machine learning framework for non-invasive arterial stiffness risk screening and cuffless BP estimation. By employing a FreeRTOS-managed ESP32 microcontroller alongside a four-stage LM324 analog front-end, strict temporal synchronization and $>$ 150 Hz broadband noise attenuation were achieved on a prototype costing under $38 USD. When evaluated on an in-silico dataset of 4,328 noise-augmented virtual subjects, the XGBoost inference engine achieved 91.22% accuracy (0.9826 macro ROC-AUC) for arterial stiffness classification and satisfied numerical AAMI and BHS Grade A margins for BP estimation (MAE $<$ 4.0 mmHg). Future work will focus on fabricating a shielded multi-layer PCB to reduce skin-contact 50 Hz capacitive coupling and conducting formal clinical trials under institutional ethics protocols to calibrate and validate the models against gold-standard cfPWV and oscillometric references across human cohorts.

References

[1] World Heart Federation, "World heart observatory: Nepal," 2026, accessed: Jun. 14, 2026. [Online]. Available: https://world-heart-federation.org/world-heart-observatory/countries/nepal/.

[2] World Health Organization, "Cardiovascular diseases (CVDs)," 2026, accessed: Jun. 14, 2026. [Online]. Available: https://www.who.int/news-room/fact-sheets/detail/cardiovascular-diseases-(cvds).

[3] C. Vlachopoulos, K. Aznaouridis, and C. Stefanadis, "Prediction of cardiovascular events and all-cause mortality with arterial stiffness: a systematic review and meta-analysis," *Journal of the American College of Cardiology*, vol. 55, no. 13, pp. 1318–1327, 2010.

[4] P. Salvi, F. Valbusa, A. Kearney-Schwartz, C. Labat, A. Grillo, G. Parati, and A. Benetos, "Non-invasive assessment of arterial stiffness: Pulse wave velocity, pulse wave analysis and carotid cross-sectional distensibility: Comparison between methods," *Journal of Clinical Medicine*, vol. 11, no. 8, p. 2225, 2022.

[5] J. Park, H. S. Seok, S.-S. Kim, and H. Shin, "Photoplethysmogram analysis and applications: An integrative review," *Frontiers in Physiology*, vol. 12, p. 808451, 2021.

[6] S. Kim, X. Xiao, and J. Chen, "Advances in photoplethysmography for personalized cardiovascular monitoring," *Biosensors*, vol. 12, no. 10, p. 863, 2022. [Online]. Available: https://www.mdpi.com/2079-6374/12/10/863

[7] P. H. Charlton, B. Paliakaitė, K. Pilt, M. Bachler, S. Zanelli, D. Kulin, J. Allen, M. Hallab, E. Bianchini, C. C. Mayer, D. Terentes-Printzios, V. Dittrich, B. Hametner, D. Veerasingam, D. Žikić, and V. Marozas, "Assessing hemodynamics from the photoplethysmogram to gain insights into vascular age: a review from VascAgeNet," *American Journal of Physiology. Heart and Circulatory Physiology*, vol. 322, no. 4, pp. H493–H522, 2022.

[8] P. H. Charlton, J. Mariscal Harana, S. Vennin, Y. Li, P. Chowienczyk, and J. Alastruey, "Modeling arterial pulse waves in healthy aging: a database for in silico evaluation of hemodynamics and pulse wave indexes," *American Journal of Physiology. Heart and Circulatory Physiology*, vol. 317, no. 5, pp. H1062–H1085, 2019.

[9] L. d. R. Mikael, A. M. G. d. Paiva, M. M. Gomes, A. L. L. Sousa, P. C. B. V. Jardim, P. V. d. O. Vitorino, M. B. Euzébio, W. d. M. Sousa, and W. K. S. Barroso, "Vascular aging and arterial stiffness," *Arquivos Brasileiros De Cardiologia*, vol. 109, no. 3, pp. 253–258, 2017.

[10] T. C. Margain, E. Powell, A. Clark, and A. Bush, "Phonocardiography based pulse wave velocity system for non-occlusive assessment of arterial stiffness," *Frontiers in Cardiovascular Medicine*, vol. 12, p. 1481836, 2025. [Online]. Available: https://pmc.ncbi.nlm.nih.gov/articles/PMC11798789/

[11] K. Pilevar Abrisham, K. Alipour, B. Tarvirdizadeh, and M. Ghamari, "Noninvasive assessment of arterial stiffness using photoplethysmography: Feature analysis and machine learning-based estimation of carotid-femoral pulse wave velocity," *IEEE Access*, vol. 13, pp. 185 657–185 673, 2025.

[12] K. Takazawa, N. Tanaka, M. Fujita, O. Matsuoka, T. Saiki, M. Aikawa, S. Tamura, and C. Ibukiyama, "Assessment of vasoactive agents and vascular aging by the second derivative of photoplethysmogram waveform," *Hypertension*, vol. 32, no. 2, pp. 365–370, 1998.

[13] B. Williams, G. Mancia, W. Spiering, E. Agabiti Rosei, M. Azizi, M. Burnier *et al.*, "2018 ESC/ESH guidelines for the management of arterial hypertension," *European Heart Journal*, vol. 39, no. 33, pp. 3021–3104, 2018.

[14] Association for the Advancement of Medical Instrumentation, "Non-invasive sphygmomanometers—part 2: Clinical investigation of intermittent automated measurement type," Association for the Advancement of Medical Instrumentation, Arlington, VA, USA, Tech. Rep. ANSI/AAMI/ISO 81060-2:2019, 2019.

[15] E. O'Brien, J. Petrie, W. Littler, M. de Swiet, P. L. Padfield, D. G. Altman, M. Bland, A. Coats, and N. Atkins, "The British Hypertension Society protocol for the evaluation of blood pressure measuring devices," *Journal of Hypertension*, vol. 11, no. Suppl. 2, pp. S43–S62, 1993.